DOI: 10.1113/JP276976

The postnatal development of ultrasonic vocalization-associated breathing is altered in glycine transporter 2-deficient mice

Swen Hülsmann[1,2,*], Yoshihiko Oke[3], Guillaume Mesuret[1,2], A. Tobias Latal[1,2], Michal G. Fortuna[1,2], Marcus Niebert[2], Johannes Hirrlinger[4,5], Julia Fischer[6], Kurt Hammerschmidt[6]

(1) Clinic for Anesthesiology, University Medical Center, Göttingen, Germany.

(2) Center for Nanoscale Microscopy and Molecular Physiology of the Brain (CNMPB), Göttingen, Germany.

(3) Division of Physiome, Department of Physiology, Hyogo College of Medicine, Nishinomiya, Japan

(4) Carl-Ludwig-Institute for Physiology, Faculty of Medicine, University of Leipzig, Leipzig, Germany

(5) Max Planck Institute of Experimental Medicine, Department of Neurogenetics, Göttingen, Germany

(6) German Primate Center – Leibniz Institute for Primate Research, Cognitive Ethology Laboratory, 37077 Göttingen, Germany

Short title: Breathing and ultrasound communication in GlyT2-deficient mice

*Correspondence should be addressed to:
Prof. Dr. Swen Hülsmann
Clinic for Anesthesiology,
University Hospital Göttingen,
37099 Göttingen, Germany
Phone: +49 551 399592
Fax: +49 551 399676
e-mail: shuelsm2@uni-goettingen.de

This is an Accepted Article that has been peer-reviewed and approved for publication in the The Journal of Physiology, but has yet to undergo copy-editing and proof correction. Please cite this article as an 'Accepted Article'; doi: 10.1113/JP276976.

Key Points

- Newborn mice produce ultrasonic vocalization to communicate with their mother.
- The neuronal glycine transporter (GlyT2) is responsible for efficient loading of synaptic vesicles in glycinergic neurons.
- Mice lacking GlyT2 develop a phenotype that resembles human hyperekplexia and die in the second postnatal week.
- Here we show that GlyT2-knock out mice do not acquire adult ultrasonic vocalization-associated breathing patterns.
- Despite the strong impairment of glycinergic inhibition they can produce sufficient expiratory airflow to produce ultrasonic vocalization.
- As mouse ultrasonic vocalization is a valuable read-out in translational research, these data are highly relevant for a broad range of research fields.

Abstract

Mouse models are instrumental in elucidating the genetic basis and neural foundations of breathing regulation. To test the hypothesis that glycinergic synaptic inhibition is required for normal breathing and proper post-inspiratory activity, we analyzed breathing and ultrasonic vocalization (USV) patterns in neonatal mice lacking the neuronal glycine transporter (GlyT2). GlyT2-KO mice have a profound reduction of glycinergic synaptic currents already at birth, develop a severe motor phenotype and survive only until the second postnatal week. At this stage, GlyT2-KO mice are smaller, have a reduced respiratory rate and still display a neonatal breathing pattern with active expiration for the production of USV. In contrast, WT mice acquire different USV-associated breathing patterns that depend on post-inspiratory control of air flow. Nonetheless, USVs *per se* remain largely indistinguishable between both genotypes. We conclude that GlyT2-KO mice, despite the strong impairment of glycinergic inhibition, can produce sufficient expiratory airflow to produce ultrasonic vocalization.

Introduction

The neuronal mechanisms of network activity that underlie the fundamental process of breathing are still not completely understood. While it is accepted that excitatory neurons in the preBötzinger Complex (preBötC) are indispensable for generation of the underlying rhythm (Gray *et al.*, 2001; Tan *et al.*, 2008; Vann *et al.*, 2016), the role of inhibitory neurons is disputed (Richter & Smith, 2014; Feldman & Kam, 2015). Pharmacological blockade of synaptic inhibition has produced contradictory results, ranging from complete loss of rhythmic activity (Pierrefiche *et al.*, 1998) or major perturbations of respiratory rhythm and pattern (Marchenko *et al.*, 2016) to only subtle alteration of frequency and amplitude (Janczewski *et al.*, 2013; Cui *et al.*, 2016; Baertsch *et al.*, 2018).

To investigate the role of inhibition for normal breathing without influence of anesthetic agents, transgenic animal models with mutations in cellular components critical for synaptic inhibition have been widely used. Mice with substantial impairment of both GABAergic and glycinergic transmission are not viable (Feng *et al.*, 1998; Wojcik *et al.*, 2006; Fujii *et al.*, 2007; Rahman *et al.*, 2015). In contrast, mice with a selective reduction of glycinergic transmission develop a phenotype that resembles human hyperekplexia (Schaefer *et al.*, 2013), but can survive the first week of life. For example, in mice lacking the adult isoform of the glycine receptor (Glra1) due to a frameshift mutation (Oscillator; $Glra1^{spd\text{-}ot}$; (Buckwalter *et al.*, 1994; Kling *et al.*, 1997; Graham *et al.*, 2003)) the respiratory phenotype is very mild (Markstahler *et al.*, 2002) with subtle changes of respiratory neuron activity (Busselberg *et al.*, 2001). Since the deficit in glycinergic transmission in $Glra1^{spd\text{-}ot}$ mice depends on the downregulation of the neonatal Glra2 subunit after two weeks of life (Becker *et al.*, 1992), alterations of breathing in the first week of life have not yet been addressed.

Mice lacking the neuronal glycine transporter (GlyT2; *slc6a5*) develop the hyperekplexia-like phenotype earlier than $Glra1^{spd\text{-}ot}$ mice (Gomeza *et al.*, 2003). Moreover, glycinergic synaptic transmission is already affected at birth in GlyT2-KO mice (Latal *et al.*, 2010). We therefore reconsidered GlyT2-KO mice as a model for the analysis of the impact of impaired glycinergic synaptic transmission on breathing behavior during the first two weeks of postnatal development. Since glycinergic inhibition is postulated to be required for post-inspiratory activity and thus, vocalization (Dutschmann *et al.*, 2014; Richter & Smith, 2014), we extended our analysis to assess the postnatal development of ultrasonic vocalization (USV).

The aim of the study was to identify potential alterations of breathing pattern related to the reduction of synaptic glycinergic inhibition in GlyT2-KO mice. As vocalization and respiration are closely linked motor activities, we also investigated, for the first time, how the interdependence of vocalizations and breathing patterns develops during the first two weeks of postnatal development.

Methods

Ethical approval

All experiments were performed in accordance with the directives for the welfare of experimental animals issued by the European Communities Council 86/609/EEC and 2010/63/EU and the German Protection of Animals Act (TierSchG). All procedures were conducted in agreement with § 4 Abs. 3 TierSchG (German Animal Protection Act) and were approved and registered (T12/11) by the animal welfare office and commission of the University Medical Center Göttingen. All investigators understand the ethical principles of "The Journal of Physiology" and the work complies with the animal ethics checklist (Grundy, 2015).

Handling of animals

Mice were bred in the animal facility of the University Medical Center Göttingen and kept under a 12h light: 12h dark cycle. Adult mice had access to food and water *ad libitum,* neonatal mice were fed by their mothers. After measurement of breathing using unrestrained whole-body plethysmography or a piezoelectric transducer (see below) mice were deeply anesthetized with isoflurane (1-2 mL in a 4 L chamber) until loss of their paw withdrawal reflex and decapitated rapidly, followed by removal of the brain for the preparation of acute brain slices (see details of preparation below). Mice that were not used for brain slices received an overdose of the anesthetic before decapitation.

Experimental design

Blinding of the experiments was not possible, since GlyT2-deficient mice (GlytT2-KO) had a white fur, and therefore were readily recognizable (Figure 1A). This mouse line was generated on a 129/OLA background (Gomeza *et al.*, 2003). The knock-out genotype and the fur color are linked because both the GlyT2 (s*lc6a5*) gene (Bogdanik *et al.*, 2012) and coat color genes (Simpson *et al.*, 1997) are located on chromosome 7. We also crossbred the line with a transgenic line (Tg(Slc6a5-EGFP)1Uze) that expressed the enhanced green fluorescent protein (EGFP) under the GlyT2-promoter (Zeilhofer *et al.*, 2005). This allowed us to identify inhibitory neurons in the slices preparations (see below). Heterozygous mice were excluded from further analysis after genotyping.

Genotyping

GlyT2-EGFP transgenic mice (Zeilhofer *et al.*, 2005) were genotyped by PCR using the primers 5'-GCCGCTACCCCGACCAC-3' and 5'-AGCATACGTGCACCCGCCAGG-3' spanning from the GlyT2 sequence to the EGFP open reading frame. GlyT2 knockout animals (Gomeza *et al.*, 2003) were genotyped as described using the primers WT1 5'-CCTCTTCTGCCTTTTTTGAGACTG-3' and WT2 5'-ATAGCCCCCACAGCATTCATCCTG-3' for

detection of the wild type allele as well as the primers KO1 5'-CAGCTCATTCCTCCCACTCATGAT-3' and KO2 5'-AGCATGCCTAGTACAACTCGA-3' for the knock out allele. However, as the exon, which is deleted in GlyT2 knock-out mice is present in the GlyT2-EGFP BAC construct, this strategy could not be used to genotype GlyT2- KO mice in the presence of the GlyT2-EGFP transgene. Therefore, these mice were genotyped using quantitative PCR by quantifying the number of neo-cassettes of the knockout allele present in the genome to discriminate GlyT2+/- from GlyT2-/- mice. Genomic DNA was isolated from tail tips of mice by the Invisorb® Spin Tissue Mini Kit (Stratec). Purified DNA (50 ng) was subjected to qPCR in triplicates, using the following primers: GlyT2-KO-s: 5'-GCTTGGGTGGAGAGGCTATT-3', GlyT2-KO-as: 5'-CATCAGAGCAGCCGATTGT-3'. The gene of neuregulin-1 was used as a reference (primer NR-s: 5'-GTGTGCGGAGAAGGAGAAAACT -3'; NR-as: 5'-AGGCACAGAGAGGAATTCATTTCTTA -3'). Real-Time-PCR was performed on a LightCycler 480 (Roche) using the LightCycler 480 SYBR Green I Master (Roche). Data were evaluated using the E-method (Roche) based on ΔΔCt –method and comparison to samples of known genotype.

Unrestrained whole-body plethysmography

Breathing and vocalization was measured within 60 min after removal from the litter. Mice could freely move and remained in the chamber (volume 280 ml; Figure 1B) during the measurement (3 min). Whole-body plethysmography utilizes the pressure changes resulting from the warming of the inspired air and cooling during expiration (Drorbaugh & Fenn, 1955). Here, we used a chamber in the so called flow-through configuration, which utilizes the principle of a pneumotach (Zhang *et al.*, 2014; Hülsmann *et al.*, 2016). In detail, the pressure difference between the recording chamber (280 ml) and a reference chamber was captured by a DP103-12 pressure transducer (Validyne Engineering) and passed through a sine wave carrier demodulator (CD-15, Validyne Engineering) for digitization (1 kHz sampling rate) with an analog-digital interface (PowerLab/4s) and LabChart-software (ADInstruments). The pressure sensor can detect very small pressure changes (± 0.008 psid). The time constant of the pressure decay from the system was 10 ms. A negative bias flow of 150 ml·min^{-1} was introduced using a CO_2/O_2 sensor (Adinstruments) to calibrate the flow signal at room temperature (two point calibration; LabChart). Since chamber temperature and humidity was not measured, we did not perform further corrections for these parameters. The raw flow signal was band pass filtered off-line (0.5 – 20 Hz), to remove movement artifacts and noise, and then integrated for the estimation of tidal volume. We used the standard integral settings of the "Integral Channel Calculation module" of the LabChart-software (use of all data points, reset each cycle whereby the integral is reset each time the source signal passes through zero to a positive value).

The peak detection module of LabChart was used to identify respiratory parameters including time of peak, tidal volume (integrated flow), peak expiratory as well as peak

inspiratory flow (table 1), which were analyzed offline. The respiratory rate was calculated as the reciprocal of the averaged peak to peak interval. Intervals that were longer than 750 ms were considered as pauses, calculated as pauses per minute. Irregularity scores (IrrScore) were calculated to assess the cycle-to-cycle variability of the interval (int) as $IrrScore_{Int} = 100 \cdot |(Int_{(n)} - Int_{(n-1)})/Int_{(n-1)}|$ and of the tidal volume (V_T) as $IrrScore_{VT} = 100 \cdot |(V_{T(n)} - V_{T(n-1)})/V_{T(n-1)}|$ (Barthe & Clarac, 1997; Wegener *et al.*, 2014; Mesuret *et al.*, 2018). To estimate the overall variability of the breathing, the coefficient of variation (CV) were calculated for V_T and respiratory cycle length (interval).

Offline calculations were performed using Excel (Microsoft). To quantify the relative number of breathing cycles with augmented expiratory flow that are characteristic for the neonatal vocalization an algorithm in Excel was developed, which defines a respiratory cycle as neonatal vocalization-like (NVL) if (i) the peak amplitude was increased (> 1.2 times average peak amplitude) and (ii) the expiratory flow measured at least 80% of the peak inspiratory flow of the same respiratory cycle.

Recording of ultrasonic vocalization

For simultaneous measurement of vocalization and breathing, an ultrasound (US) microphone (UltraSoundGate 116H; Avisoft Bioacoustics) was incorporated into the lid of the plethysmography chamber (Figure 1B). US signals were recorded and digitized using chart software (40000 Hz sampling rate) to determine their timing with respect to the respiratory cycle and Avisoft recorder software (Avisoft Bioacoustics) for detailed spectral analysis. The distance between the animal and the US microphone was about 20 mm while the distance to the pressure sensor was about 200 mm causing a short delay of pressure signal (0.5 ms). With respect to a respiratory cycle length of approximately 200 ms (@ 300 BPM) and filtering we refrained from correction of timing during our data analysis.

Brainstem slices preparations

WT and GlyT2-KO mice (P1-P9) were deeply anesthetized with isoflurane (1-2 mL in a 4 L chamber) until loss of their paw withdrawal reflex and decapitated rapidly to remove the brain. The brainstem was isolated, mounted on an agar-block and transferred to a vibratom (VT1200S, Leica). In carbogenated (95% O_2, 5% CO_s) aCSF (containing in mM: 118 NaCl, 3 KCl, 1.5 $CaCl_2$, 1 $MgCl_2$, 1 NaH_2PO_4, 25 $NaHCO_3$, and 30 D-glucose (330 $mosmol \cdot l^{-1}$; pH 7.4) transversal slices were cut until the level of the principle nucleus of the inferior olive was reached. Then a 550-600 µm thick slice containing the preBötC was cut. This slice was transferred to the recording chamber to be superfused with aCSF. Temperature was raised to 28°C and the external potassium-concentration increased to 8mM. The local field potential was recorded with borosilicate glass-electrodes from the preBötC (Zhao *et al.*, 2006). Recordings were amplified 5,000-10,000 times, band-pass filtered (0.25-1.5 kHz), rectified and integrated (Paynter filter with a time constant of 40-70 ms). The digitized signal

(at 10 KHz; Digidata 1440) was visualized and stored by pCLAMP 10 software (Molecular Devices).

Two-photon excitation microscopy and calcium Imaging

We used a two-photon microscope (TriMScope, LaVision BioTec) with non-descanned detection by Hamamatsu GaAsP photomultipliers. Settings were controlled by "Imspector pro" software (LaVision BioTec). Excitation was achieved with a Ti:Sapphire Laser (SpectraPhysics MaiTai BB) at 800 nm for OGB-1-AM and 900 nm for EGFP. As described previously (Winter *et al.*, 2009; Schnell *et al.*, 2011) fluorescence signals of EGFP were detected through a 475/50 nm band pass filter, whereas OGB-1-AM was excited with detected through a 531/40 nm band pass filter (AHF Analysentechnik AG).

For labelling cells with calcium indicator dye (Oregon green BAPTA-1 AM; OGB1-AM), multi-cell bolus loading was used (Stosiek et al., 2003). Briefly, AM-ester of OGB1 (50 µg; Molecular Probes) was dissolved in 40 µl DMSO containing 20% Pluronic F-127 (Molecular Probes) as OGB-stock solution and stored at -20°C until usage. A pipette solution for injection was prepared containing in mM: 150 NaCl, 2.5 KCl, 10 Hepes; pH 7.4. 4 µl of the OGB-stock solution was added to 16 µl of injection-solution, resulting in a final dye concentration of 200 µM. Approximately 2 µl of the final injection-solution were filled in a patch-pipette (resistance 3-5MΩ) and pressure-injected (0.7 bar; 60 s) into the slice. Calcium imaging of neuronal activity was performed on the same side of the slice where the local preBötC field potentials were recorded. To estimate the number of respiratory neurons, rhythmic calcium signaling was recorded in different depths of the slice (between 20 µm and 120 µm, at a step size of 10 µm). Time lapse images (250 µm x 250 µm) were acquired at a rate of 10 Hz. For each imaging plane both the number of EGFP-positive glycinergic neurons and the fraction of rhythmic EGFP-positive glycinergic neurons was determined. For each slice the averaged number per plane was calculated. Data were stored on Windows PCs for offline analysis. Calculation of cross correlation maps and cycle triggered averaging was performed by customized macros using Matlab® (Mathworks; see (Winter *et al.*, 2010; Schnell *et al.*, 2011)).

Analysis of ultrasonic vocalization (USV)

The sampling frequency of 250 kHz resulted in a frequency range of 125 kHz. We used the whistle tracking algorithm of Avisoft-SASLab Pro 5.2 (Avisoft Bioacoustics) with following settings: monotonic, maximum change per step 8 pix = 3.9 kHz, minimum continuity = 8ms, hold time = 15ms. As sound energy outside the frequency range of the produced USVs can have a negative influence on the estimations, we applied a high pass FIR filter of 35 kHz. In addition, we checked visually the outcome of the whistle tracking procedure because in some cases the program selected other sounds such like toe clicking, sniffing or high frequency background sounds erroneously as USVs. These criteria were compared with

former studies of pup vocalizations (Hammerschmidt *et al.*, 2012; Hammerschmidt *et al.*, 2015). Based on these settings we calculated the number of given call elements and the latency to start calling.

For a subtle acoustic characterization of USVs, we calculated high-resolution spectrograms from the stored call elements (FFT=1024, frequency range: 125 kHz, frequency resolution: 244 Hz, time resolution: 0.26 ms) and submitted the resulting spectrograms to the custom software program LMA 2017 to extract characteristic acoustic parameters (for further details see Fischer *et al.*, 2013; Hammerschmidt *et al.*, 2015). As mice typically concentrate the energy into one small frequency band, so-called ‘‘whistles’’ or ‘‘pure tone-like sounds’’, we focused our estimations on the peak frequency (PF), the frequency with the highest amplitude in the spectra (Figure 1D). Often mice produce soft USVs and already minor head movements can lead to amplitude fluctuations. Therefore, we visually controlled the acoustic parameters and excluded incorrectly estimated calls from the analysis. For each element, we estimated the duration. We defined the start of an element if the sound energy of a time segment exceeds 10% of the mean maximum amplitude of this element. We used the same threshold (10%) to determine the end of an element. In addition, we calculated parameters describing the level and modulation of PF (Hammerschmidt *et al.*, 2012). As many of these parameters could show high correlation we used a step-wise discriminant function analysis (SPSS 24) to reveal which of these parameters are most helpful to distinguish between KO and WT littermates. As two of the 39 subjects did not produce any USVs we could include 3622 USVs from 37 subjects in this comparison.

USVs in relation to respiratory flow

To estimate differences in the respiratory flow between cycles with and without USVs we marked every cycle with USVs. In addition, we marked for a subset of clear loud vocalization the exact start time of the vocalization in relation to the respiratory flow. To make this comparison we used the channel with the additional recording of the ultrasound signal at 40 kHz sampling frequency (see above, Figure 1C). Only those animals, which produced more than 10 calls during the 3 min window, were used for this analysis.

- Figure 1 -

Video capturing and recordings of abdominal movements

During USV forced abdominal movements can be observe (see supplementary video). The video capture feature of LabChat 8 was used together with USB WEB-camera (30 Hz frame rate; Philips SPC520NC). Synchronization between camera and analog input signals were adjusted manually using Labchart8 software and tested by light pulses from a LED (470 nm; KSL 70; Rapp OptoElectronic). Additional, USV-signal from the ultrasound (US) microphone

(UltraSoundGate 116H; Avisoft Bioacoustics) was recorded with labchat8 at a sampling rate of 40Hz (lower trace in supplementary video).

Since the video rate of our camera was relatively low, we had to consider aliasing problems when interpreting the video. To overcome this problem, we combined the video capturing with direct recordings of abdominal movements, using a piezoelectric transducer (PZT; FT31T1.3A1472; KEPO). Therefore, pups were placed with their belly on the PZT element. An increase of the pressure on the PZT is recorded as an upstroke of the recording trace. Piezoelectric signals (upper trace in video) were collected at a sampling rate of 40 kHz using Labchart8 software without amplification using a PowerLab 4/35 interface that was connect to Fujitsu Q704 computer. The final video is a screen recording using the Microsoft Windows 10 onboard video capture option.

Calibration of the PZT-recordings of abdominal movements and the plethysmography flow signal

To calibrate the timing of the PZT-recordings of abdominal movements and the plethysmography signal, the mouse was placed on the PZT within the plethysmography chamber and flow signal (Figure 1E and F; upper trace) and the PZT-signal (middle trace) were recorded together with USV-signal (lower trace) at 40Hz sampling rate (LabChart8; PowerLab 4/35).

Statistical analyses

To test for difference in relation to genotype and age, we first used the general linear model (GLM univariate analysis of variance) of IBM SPSS 24 with genotype (WT, GlyT2-KO) and age (P0-3, P4-7, P8-12) as fixed factors. For age, we conducted a post hoc test (LSD equal variance assumed). In case of violated test assumptions or significant interaction between genotype and age, we conducted separate nonparametric tests (Mann-Whitney U-Test, Kruskal-Wallis One Way ANOVA). For the comparison of acoustic parameters we calculated the mean per subject and used these to conduct the GLMs. For the comparison of the results from the slice experiments, we employed Mann-Whitney U tests.

To take account for the relatively small number of animals per age group, we report the actual effect size for all significant tests: “Partial eta squared” (η^2) for GLM tests and “Pearson’s r” for Mann-Whitney U-tests. Data in the manuscript are presented as median. Additionally the interquartile range (IQR) is provided.

Results

Development of breathing pattern in GlyT2-deficent mice

In the first set of experiments, we analyzed the breathing phenotype of GlyT2-KO mice at different stages during postnatal development. We therefore separated the mice into three age groups comprising postnatal days P0-3, P4-7 and P8-12.

- Figure 2 -

In the first age group (P0-3, Figure 2A, Table 1), no differences were observed between GlyT2-KO mice and WT littermates in respiratory rate (fR). The median of the respiratory rate was 148 min^{-1} in GlyT2-KO mice (interquartile range (IQR): 141-157 min^{-1}; n=7) and 163 min^{-1} (143-167 min^{-1}; n=9) in WT littermates (Mann–Whitney U-test, U=38, p=0.491; Figure 2E). In both genotypes, we found respiratory pauses (>750 ms), but no difference between the genotypes (Figure 2G). Tidal volume (V_T; Mann–Whitney U-test: U=62, p<0.001, r=0.81) and minute ventilation (V_e; Mann–Whitney U-test: U=61, p<0.001, r=0.78) of GlyT2-KO mice were, however, significantly lower than in WT mice. While V_T of WT was 0.25 µl (0.23-0.3 µl), V_T of GlyT2-KO mice was 0.11 µl (0.12-0.15 µl; Figure 2F). V_e of WT was 39.6 µl·min^{-1} (34.5-44.1 µl·min^{-1}), V_e of GlyT2-KO mice was 21.6 µl·min^{-1} (18.3-26.2 µl·min^{-1}; Figure 2H). Next, we analyzed the occurrence of high amplitude respiratory cycles. These are characterized by an increase of inspiratory and particularly expiratory air flow (see Methods). Such intermittent alterations of breathing have been shown to be related to USV (Hodges *et al.*, 2009; Hernandez-Miranda *et al.*, 2017). We refer to these alterations of breathing as 'neonate vocalization-like' (NVL) cycles. At P0-3, WT mice produced NVL cycles in 16.5 % (11.1-20.1 %) of all observed cycles, while in GlyT2-KO 6.4 % (5.5-13 %) of all cycles were NVL cycles; the difference was highly significant (Mann–Whitney U-test: U=51, p=0.002, r=0.78; Figure 2D). This observation suggests that differences in tidal volume and thus, minute ventilation reported above are related to differences in vocalization.

- Table 1 -

In the second age group (P4-7, Figure 2B, Table 1), *f*R of WT mice increased to 286 min^{-1} (214-310 min^{-1}; n=6) and to 177 min^{-1} (168-192 min^{-1}; n=12) in GlyT2-KO mice. This difference between the genotypes was statistically significant (Mann–Whitney U-test: U=69, p=0.001, r=0.73). In this age group, no significant alterations were detected between genotypes regarding V_T and V_e. Longer pauses (> 750 ms) were only found in GlyT2-KO mice (0.46 min^{-1} (0.01-4.3 min^{-1})). Compared to the first age groups, V_e increased in both WT and GlyT2-KO mice at P4-7 (WT mice: 178 µl·min^{-1} (115-237; n=6) vs. GlyT2-KO mice: 86.8 µl·min^{1} (60.7-209; n=12)). Again, the most prominent distinction was the variation in NVL cycles. However in this age group, WT mice (3.2 % (2.5-7.8%) showed less NVL cycle as compared to GlyT2-KO mice (26.1% (10-31%); Figure 2D).

In the last age group (P8-12, Figure 2C, Table 1), the disparity in breathing phenotype between WT and GlyT2-KO mice became even more obvious. Strikingly, GlyT2-KO mice still showed NVL breathing in 24.3 % (13.7-28.3 %) of the cycles (n=17; Figure 2D), while WT littermates (n=12) showed NVL breathing in only 3.2 % (1.4-3.9 %) of the cycles (Mann–Whitney U-test: U=3, p<0.001, r=0.81). Moreover, *f*R was significantly lower in GlyT2-KO mice (171 min^{-1} (149-205 min^{-1}; n=17)) compared to WT mice (319 min^{-1} (279-336 min^{-1}; n=12; Mann–Whitney U-test: U=204, p<0.001, r=0.84; Figure 2E). Long pauses (> 750 ms) were again only found in GlyT2-KO mice (0.65 min^{-1} (0.2-2.7 min^{-1}; Figure 2G)). In this age group, V_e of GlyT2-KO mice remained at the level of the first week (120 µl·min^{-1} (79.1-182 µl·min^{-1}; n=17)), while V_e in WT mice increased to 309 µl·min^{-1} (262-464 µl·min^{-1}; n=12). The difference between genotypes was highly significant (Mann–Whitney U-test=199, p<0.001, r=0.8; Figure 2H).

Taken together, it appears that breathing of GlyT2-KO mice did not mature and remained at a neonatal level. This was not only reflected by the number of respiratory cycles with high expiratory air-flow, but also by the persistence of high numbers of pauses in GlyT2-KO mice. Both of these characteristics disappeared over time in WT mice.

Interestingly, when correcting V_e for body weight (V_e/BW), the differences between genotypes at P8-12 disappeared (Figure 3, Table 1), suggesting that the lighter GlyT2-KO mice might still reach sufficient ventilation to meet the metabolic demands.

- Figure 3 -

Generation of neuronal activity in the pre-Bötzinger Complex is not impaired in GlyT2-KO mice

To test if the breathing phenotype is due to an alteration of the brainstem network in the preBötC (Smith *et al.*, 1991) that generates respiratory rhythm, we performed recordings from rhythmic brainstem slices (Age P1-9). Since analysis of respiratory activity in this type of slices using pharmacological blockade of inhibition (by strychnine) revealed contradictory results for the frequency (ranging from increase (Zhao *et al.*, 2006), via no effect (Shao & Feldman, 1997) to even reduction of frequency (Baertsch *et al.*, 2018)), we aimed to test the alterations of the network activity in GlyT2-KO mice. Although the frequency of the respiratory burst activity was slightly faster in slice preparations from GlyT2-KO mice (0.09 Hz (0.06-0.17 Hz); n=6) as compared to WT littermates (0.07 Hz (0.05-0.14 Hz); n=5), the difference did not reach statistical significance (Mann-Whitney U-Test: U = 11.00, P = 0.537; Figure 4). The irregularity score of the interburst interval was not significantly different either (WT 0.97 (0.59-1.3); GlyT2-KO 1.2 (0.55-3.8); Mann-Whitney U-Test = 12.00, P = 0.662). Additionally, we performed calcium imaging of the preBötC in respiratory slices. We did not find differences between WT and GlyT2-KO mice in respect to the number of active respiratory neurons (Mann-Whitney U-test: U=5.5, p=0.171) nor between the relative

numbers of glycinergic respiratory neurons (Mann-Whitney U-test: U=10, p=0.762; Figure 4). These data, the absence of differences in *in-vitro* recordings, lower body weight (Table 1) and immature vocalization-like breathing, strongly suggest that there is no primary defect in the central respiratory rhythm generating network of the preBötC that accounts for the observed alteration in GlyT2-KO mice.

- Figure 4 -

Differences in vocal activity

To identify potential alterations of USV due to variation in respiratory patterns, we analyzed the production of USVs in more detail. The total number of USVs increased over development (general linear model (GLM): F_2=13.1, p<0.001, η^2=0.442; Figure 5A), but there was no significant differences between WT and GlyT2-KO mice (GLM: F1=2.4, p=0.128). WT mice from the first age group (P0-3) produced 38 calls·min^{-1} (6.8-62 calls·min^{-1}; n=9) and GlyT2-KO mice produced 13.7 calls·min^{-1} (8-21.4 calls·min^{-1}; n=6). One mouse of each genotype did not produce any call during the time of observation. Although this higher activity in WT fits well with the higher number of NVL cycles observed before, this difference was not significant. In the second age group, no differences were observed. In the third age group (P8-12), WT mice produced 100 calls·min^{-1} (82-118 calls·min^{-1}; n=7) and GlyT2-KO littermates 54 calls·min^{-1} (21-116 calls·min^{-1}; n=7; Figure 5).

The increase of USV-calls with age probably could be explained by the observation that the latency to call (after placement in the chamber) decreased between P0-3 and P8-12 (GLM: F_2=7.6, p=0.002, η^2=0.323; Figure 5B). There was no significant difference between WT and GlyT2-KO (GLM: F_1=0.43, p=0.519).

- Figure 5 -

Analysis of the acoustic structure of USVs

Next we aimed to analyze the acoustic structure of the USV in more detail. The step-wise discriminant function used 15 out of 39 acoustic parameters (Fischer *et al.*, 2001) to assign the pup isolation calls to the genotypes (correct classification=63.4%, cross-validated=63%), which is only a little above chance level (50%). Thus, in general, GlyT2-KO and WT mice differed only marginally in the structure of their USVs (Figure 6A,B).

GlyT2-KO mice produced USVs with a significantly shorter call duration (GLM: F_1=5.1, p=0.032, η^2=0.141; Figure 6C) across all age categories, but there was no difference in call duration between age groups (GLM: F_2=0.7, p=0.497). The only other significant effect was a change in peak frequency during development, with a higher peak frequency in older mice (GLM: F_2=13.8, p<0.001, η^2=0.471; Figure 6D). No substantial difference between genotypes was detected for this parameter (GLM: F_1=2.8, p=0.107). We also found no significant

differences in the other acoustic parameters in relation to genotype or age (Figure 6E,F): Frequency range, genotype (GLM: F_1=0.3, p=0.617); Frequency range, age (GLM: F_2=0.2, p=0.821); slope, genotype (GLM: F_1=2.1, p=0.155); slope, age (GLM: F_1=1.8, p=0.189).

- Figure 6 –

Differences in ventilation in relation to vocalization events

As shown above, GlyT2-KO mice had a different respiratory pattern compared to WT littermates. The respiratory pattern is assumed to be related to USV. We therefore analyzed, whether the observed alterations of ventilation are directly associated with variation in USV.

We observed a lower peak inspiratory flow in GlyT2-KO mice at P8-12, both in respiratory cycles associated with a call (Figure 7A) as well as in cycles that were not associated with a call (Figure 7B; GLM (WT vs. GlyT2-KO) cycles followed by USV: F_1=28.8, p<0.001, η^2=0.545; cycles not followed by USV: F_1=42.2, p<0.001, η^2=0.638), indicating that the reduction of minute ventilation at this stage is only partially related to the variation in the number of calls but also an effect of a reduction of tidal volume during respiratory cycles with USV.

Comparing the changes in inspiratory flow during USV and in cycles without USV, we found a higher inspiratory flow in respiratory cycles with USV in all subjects (Figure 7C). Older mice showed a more prominent increase in inspiratory flow than younger mice (GLM: F_2=7.5, p=0.003, η^2=0.384). However, there was no significant difference between genotypes (GLM: F_1=0.28, p=0.601), indicating that GlyT2-KO mice are able to control and alter inspiratory neuronal activity in a coordinated manner.

At birth, USV-calls are associated with active expiration (Hernandez-Miranda *et al.*, 2017) and thus, with an increase of airway pressure and expiratory flow. Moreover, it is suggested that the peak frequency of USVs depends on the speed of the expiratory airflow (Mahrt *et al.*, 2016). To assess whether the control of expiratory air flow is impaired in GlyT2-KO mice, we next compared the expiratory peak flow during cycle with and without USV (Figure 7D-F).

In neonatal mice (P0-3), we found significant differences between WT and GlyT2-KO mice in the peak expiratory flow during cycles without vocalization (Mann–Whitney U-test: U=20, p =0.016, r=0.77). During development, the peak expiratory flow in respiratory cycles without vocalization increased significantly in both genotypes (GLM: F_2=35.7, p<0.001, η^2=0.748) and this increase was significantly larger in WT mice than in GlyT2-KO mice (GLM: F_2=44.4, p<0.001, η^2=0.649; Figure 7E).

In call-related respiratory cycles, no differences could be detected between the genotypes (GLM: F_1=0.16, p=0.692). However, expiratory peak flow increased from birth (P0-3; WT 6.5

µl·s^{-1} (5.8-6.7 µl·s^{-1}; n=6) vs. GlyT2-KO 6.4 µl·s^{-1}; n=3) to the second postnatal week (P8-12: WT 17.9 µl·s^{-1} (14.3-19.5 µl·s^{-1}); n=7) vs. GlyT2-KO 12.8 µl·s^{-1} (9.8-20.1 µl·s^{-1}); n= 5). Neonate mice (WT and GlyT2-KO) increased the expiratory airflow to produce ultrasonic vocalization, while WT mice in the second postnatal week (P8-P12) are producing USV-calls without an increase of expiratory flow (Figure 7F). In contrast, GlyT2-KO mice of all age group showed a significant increase in expiratory flow when producing USV-calls (GLM: F_2=24.1, p<0.001, η^2=0.668; Figure 7F). These data demonstrated that GlyT2-KO mice in the second postnatal (P8-12) week still need to utilize active expiration to produce sufficient airflow for USVs.

- Figure 7 -

The timing of the USV in relation to respiratory flow

Finally, we analyzed the timing of the USV-calls. In both genotypes, the USVs started shortly after the expiratory flow peak (Figure 8). During maturation (P4-P7 and P8-12), the start of the USVs shifted from the expiratory peak (GLM: F_2=9.3, p=0.001, η^2=0.435) to the zero flow point and the inspiration peak (Figure 8E). The changes in WT and GlyT2-KO mice were, however, different in the way that GlyT2-KO mice showed a less pronounced age-related shift than WT littermates (in relation to the zero flow point (GLM, F_1=14.9, p=0.001, η^2=0.383; Figure 8E), as well as the expiratory flow peak (GLM, F_1=15.3, p=0.001, η^2=0.391; Figure 8F)). At P8-12, USVs of WT mice started only 8 ms (0.6-14.7 ms) after the zero flow point (volume peak) but 41 ms (18-68 ms) before the expiratory peak, while in GlyT2-KO mice, USVs started 27 ms (23-31 ms) after the volume peak and just 6.7 ms (3.3-11.8 ms) before the expiratory peak (Figure 8E,F). These results not only confirm that the USV-associated breathing pattern of GlyT2-KO mice remains immature, but also suggests that in WT mice, active expiration is replaced by a post-inspiratory control of the air flow.

- Figure 8 -

Discussion

Apart from the development of the hyperekplexia-like motor phenotype (Gomeza *et al.*, 2003), symptomatic GlyT2-KO mice display a significant reduction of the respiratory rate and altered USV-associated breathing pattern.

Normal network activity in respiratory rhythmic slice preparation from GlyT2-KO mice

Respiratory rhythmic slices (Smith *et al.*, 1991; Ramirez *et al.*, 1996) have been widely used to assess alternations of network activity after manipulation of glycinergic transmission using both pharmacological intervention (Shao & Feldman, 1997; Zhao *et al.*, 2006; Baertsch *et al.*, 2018) or transgenic mice (Gomeza *et al.*, 2003; Zhao *et al.*, 2006). Pharmacological

blockade of glycine receptors has produced contradictory results. While Baertsch and colleagues (2018) reported a reduction of the frequency of network activity by strychnine, Shao and Feldman (1997) found no change in frequency. Contrarily, we have reported a significant increase of the frequency of the preBötC field potential (∫preBötC) after application of 1 µM strychnine as well as a significantly higher frequency in mutant oscillator mice (Glra1$^{spd\text{-}ot}$; (Zhao *et al.*, 2006)). These mice lack the adult isoform of the glycine receptor (Glra1) due to a frameshift mutation (Buckwalter *et al.*, 1994; Kling *et al.*, 1997; Graham *et al.*, 2003). It remains speculative why the frequency of the ∫preBötC is increased in Glra1$^{spd\text{-}ot}$ mice but not in GlyT2-KO mice. One option is that Glra1$^{spd\text{-}ot}$ mice survive longer, and thus experiments in Glra1$^{spd\text{-}ot}$ mice reflect a condition that cannot be tested in GlyT2-KO mice. Since the reduction of glycinergic transmission starts to be reduced at birth and then stays rather constant (Latal *et al.*, 2010), while in Glra1$^{spd\text{-}ot}$ mice the deficit peaks in the 3rd postnatal week (Graham *et al.*, 2003), developmental aspects might be involved. However, a compensatory effect by an increase of GABAergic transmission has been excluded for both lines (Graham *et al.*, 2003; Latal *et al.*, 2010). Complete blockade of inhibition (by bicuculline and strychnine) was found to increase the number of respiratory neurons that can be detected by calcium imaging in the slice preparation (Schnell *et al.*, 2011). Thus, our current results from the GlyT2-KO mice is in line with the concept that sufficient amount of inhibition is left to temper the network activity and to prevent over-excitation.

Early alteration of breathing in GlyT2-KO mice

Although it is generally assumed that glycinergic transmission is essential for a normal 3-phase breathing (Richter & Smith, 2014; Shevtsova *et al.*, 2014), there is experimental evidence that glycinergic inhibition is mainly relevant in feedback regulation of respiratory reflexes but dispensable for the generation of the basic respiratory rhythm (Janczewski *et al.*, 2013; Baertsch *et al.*, 2018). The presented data from GlyT2-KO mice seem to be in line with this concept. Whole cell recordings in acute slices and cell culture confirms that glycinergic transmission is severely impaired in GlyT2-KO mice (Gomeza *et al.*, 2003; Latal *et al.*, 2010). Nevertheless, respiratory activity and termination of inspiration are still functioning *in vivo*. One reason might be that a GABAergic mechanism (Dutschmann & Herbert, 2006; Arata, 2009; Barnett *et al.*, 2017) or intrinsic conductances (Zhao *et al.*, 2006; Krey *et al.*, 2010) can compensate for glycine deficiency to maintain inspiratory off-switch and thus rhythmic network activity. Interestingly, we observed a reduction of V_T and V_e (Figure 2) in GlyT2-KO mice already in the first postnatal stage (P0-3). Although this reduction might be an epiphenomenon of a lower number of USVs, other possibilities have to be considered, including a reduction of spillover of glycine to NMDA receptors at motoneurons (Berger *et al.*, 1998; Eulenburg *et al.*, 2005) or other forms of (homeostatic)

plasticity that keep the excitation-inhibition balance constant (Turrigiano & Nelson, 2004; Koch *et al.*, 2011).

USV-associated active expiration disappears in WT but not in GlyT2-KO mice

USV is vital for normal development of mice, since it is required e.g. for nesting behavior of mothers (Noirot, 1972; Noirot, 1974; Portfors, 2007). Separation from the mother induces ultrasonic vocalization (Portfors, 2007) but neither an intact cerebral cortex (Hammerschmidt *et al.*, 2015) nor a functional auditory system (Hammerschmidt *et al.*, 2012) is required for the induction of this behavior, and the neuronal mechanisms that initiate USV are not entirely understood. Since vocalization in adult mice occurs in the post-inspiratory phase of the breathing cycle (Dutschmann *et al.*, 2014; Richter & Smith, 2014) and many post-inspiratory neurons are glycinergic (Ezure *et al.*, 2003), one would expect that alterations of glycinergic inhibition are critical for the control of laryngeal muscles and thus, USV (Dutschmann & Paton, 2002; Dutschmann *et al.*, 2014). However, some investigators claim that generation of post-inspiratory activity depends on GABAergic and not glycinergic inhibition in mice (Anderson *et al.*, 2016).

Contrarily, USV in neonatal mice occurs during active expiration and requires recruitment of abdominal muscles (Hernandez-Miranda *et al.*, 2017). Active expiration is characterized by increased activity of abdominal muscles (Bianchi *et al.*, 1995). It is absent in quiet breathing but is generated, apart from vocalization, during coughing and sneezing as well as during states of high metabolic demand (Price & Batsel, 1970; Richter, 1982; Anderson & Ramirez, 2017). Active expiration requires the activity of the parafacial respiratory group (pFRG) (Onimaru & Homma, 2003; Janczewski & Feldman, 2006) and can be induced by optogenetic stimulation or pharmacological disinhibition of the pFRG *in vivo* (Pagliardini *et al.*, 2011).

Neonatal GlyT2-KO mice showed USV-associated active expiration just like their WT littermates (Figure 2A) and almost indistinguishable USV-calls (Figure 6). In the second postnatal week, however, the general characteristics of breathing and USV-associated breathing pattern of GlyT2-KO mice continued to resemble the pattern of neonates, while it matured in WT littermates. Most importantly, GlyT2-KO still showed active expiration associated with USV (Figure 1EF, Figure 2BC, supplementary video). This observation favors a dominant role of GABAergic rather than glycinergic transmission in the control of active expiration in neonates.

In contrast, WT mice developed a fundamentally altered USV-associated respiratory pattern (Figures 2C and 8C): in the second postnatal week, USV was generated almost without any increase in the expiratory flow, thus, without active expiration. Furthermore, the timing changed as USV-calls of WT mice started at the beginning of the post-inspiration (Gautier *et*

al., 1973; Richter, 1982). This change in timing of the USV-calls is in line with the concept that vocalization occurs in the post-inspiratory phase in adults (Dutschmann *et al.*, 2014; Richter & Smith, 2014).

However, it is difficult to imagine that the absence of this transition in GlyT2-KO mice is a direct consequence of the impairment of glycinergic synaptic transmission. As explained below we conclude that the different respiratory pattern during USV is rather a consequence of a general delay or impairment of postnatal development.

Functional implication of airflow on USV generation

The expiratory/post-inspiratory airflow needs to reach a critical level to produce ultrasonic vocalization (Mahrt *et al.*, 2016). Considering the smaller airway diameter of neonate mice it is not surprising, according to Hagen–Poiseuille law, that smaller and younger mice and also older GlyT2-KO must use active expiration to produce a pulmonary pressure that matches the larger airway resistance. Since older WT mice reach higher expiratory flow already during quiet breathing, USV can be generated without active expiration (Figures 2 and 8).

One of the current models of USV production concludes that USV calls are produced by intra-laryngeal planar impinging jets (Mahrt *et al.*, 2016). According to this model, the frequency of the ultrasounds calls depends on the speed of airflow, which is in line with our observation that the peak frequency of the USV calls is increasing with age and also higher in WT as compared to GlyT2-KO mice (Figure 6). Since the frequency range and slope of the USV-calls are not different between genotypes, we have no reason to believe that different physical mechanisms are utilized.

Technical consideration

As obvious from figure 1C, the raw trace shows some fluctuations of the baseline, which may result from slight changes of the bias flow or, more likely, movements of the animal. Changes of atmospheric pressure in the laboratory were blunted by the fact that we recorded pressure differences between the chamber and a reference chamber. These baseline fluctuations are largely removed by band pass filtering (0.5 – 20 Hz). However, some uncertainty remains regarding the position of the zero-flow point for each cycle, which, in principle, produces a problem for the calculation of volume data (V_T). Also, it has to be taken into account that the volume signal was not corrected for changes of humidity or temperature. We assume that these errors are random and thus, at least partially, cancel each other out. Nevertheless, some caution is advised when interpreting the absolute values of volume data (V_T and V_e).

Uncertain causality between immature breathing phenotype and early death

Although breathing of symptomatic GlyT2-KO mice is significantly different from WT littermates, there is little evidence that this alteration is directly responsible for the impaired general condition and early postnatal death. Instead, it appears that ventilation matched metabolic demands, since normalized minute ventilation ($\mu l \cdot min^{-1} \cdot g^{-1}$) is not reduced in symptomatic GlyT2-KO mice as compared to WT littermates. In GlyT2-KO mice, the increase in ventilation during vocalization might even provide a rescue mechanism for hypoxic or hypercapnic challenges that occurred during pauses as suggested for other mouse models (Hodges *et al.*, 2009). However, apneas or periods of low ventilation sometimes followed directly after periods of USV, indicating that the vigorous USV episodes might be responsible for a reduction of the respiratory drive due to functional hyperventilation during prolonged periods of USV (Figure 2B). In the long run, however, symptomatic GlyT2-KO mice might consume more energy during vocalization as their littermates because of the recruitment of expiratory muscle. Evaporative heat loss and dehydration during the vocalization might also have an adverse effect. Together with motoric difficulties to feed (Gomeza *et al.*, 2003), these alterations might lead to exhaustion of the metabolic sources and eventually decompensation. In support of this argument, our observation suggests a longer survival when litters were smaller or littermates were removed early after birth.

Conclusions

Taken together, GlyT2-KO mice have significant alterations in breathing. However, these alterations appear not immediately life-threatening. Nevertheless, an indirect relation between the early postnatal death and the deficit in glycinergic inhibition cannot be fully excluded. GlyT2-KO mice show a delayed development and consequently maintain a neonatal breathing phenotype, which is accompanied by neonatal vocalization pattern. Additionally, we show that during the first postnatal week the USV-related breathing pattern of WT mice undergoes a fundamental shift from active expiration to a post-inspiratory control of passive expiration. Finally, these findings not only contribute to a better understanding of the unclear role of glycinergic neurons in the control of breathing, but also shines new light on USV generation in general and on its postnatal development.

Figure legends

Figure 1:

Analysis of breathing and mouse ultrasonic vocalization (USV). **(A)** Appearance of GlyT2-KO mice (white fur) and WT and heterozygous littermates (black fur) at postnatal day 3 (P3) and 8 (P8): Note the growth deficit of GlyT2-KO mice as compared to littermates at P8. **(B)** Experimental setup for unrestrained whole body plethysmography and ultrasound recording. **(C)** Example traces from a neonate: 1st trace raw signal of the pressure sensor. 2nd trace from top: band pass filtered raw signal removes offset defined zero crossing; 3rd trace: integrate signal, conversion into volume information. 4th trace: ultrasound recording (40Hz sampling rate) to define timing of the USV calls. **(D)** Example spectra of pup isolation calls. **(E)** Comparison of breathing (in flow-through configuration chamber) and the abdominal movements of mice during USV. Recordings of the flow-signal (upper trace) and the signal of a piezoelectric transducer (PZT; middle trace) together with USV-signal (lower trace) from a GlyT2-KO mouse (P6). **(F)** Same recording a higher temporal resolution showing the coincidence of a drop in the PZT-signal and the expiratory peak of the flow signal, which is compatible with the concept that the expiratory flow during USV is produced by contraction of the abdominal muscles (Bianchi *et al.*, 1995).

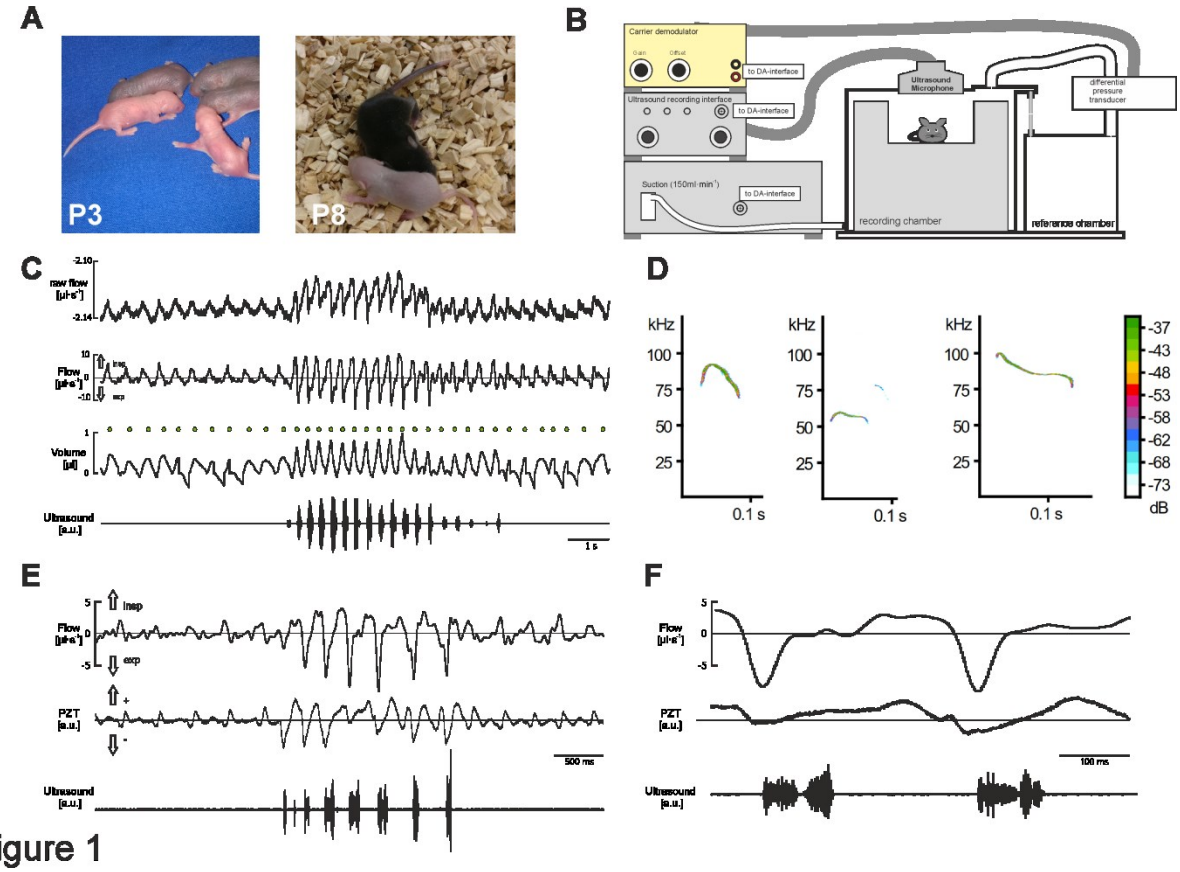

Figure 1

Figure 2:

Comparison of breathing of WT and glycine transporter 2 deficient mice (GlyT2-KO) at different developmental stages **(A)** Breathing (filtered flow) of neonatal mice (P0-3); WT (black) and GlyT2-KO (red trace). Note the increase of expiratory flow (downward deflection) during USV (vocalization-like breathing) both in WT and GlyT2-KO mice. **(B)** Recordings from WT (black) and GlyT2-KO (red trace) in the age group (P4-7). Note that the increase of expiratory flow during USV is diminished in WT mice. **(C)** Recordings from WT (black) and GlyT2-KO (red trace) in the age group (P8-12). **(D-H)** Statistical analysis of major respiratory parameters in 3 different age groups P0-3, P4-7 and p8-12 (additional parameters are shown in Table1). Median is shown by the blue line; numbers (n) of animals tested are depicted inside the boxes below the diagrams; WT: black dots and GlyT2-KO: red dots. **(D)** Neonatal vocalization-like cycle (increase of expiratory flow, see Methods). **(E)** Respiratory rate (fR; Breath per minute, BPM). **(F)** Tidal volume (V_T; µl), data from the integration of the flow signal. **(G)** Number of pauses > 750 ms. **(H)** Minute ventilation (V_e; µl·min^{-1}). Subjects presented as single data point, WT black squares, GlyT2-KO red circles, median is shown by the blue line; n= number of animals. Significant differences ($p < 0.05$) between genotype per age categories are marked as "*" (Mann-Whitney U-Test). Significant differences ($p < 0.05$) between age categories are marked as "#" (Kruskal-Wallis One Way ANOVA).

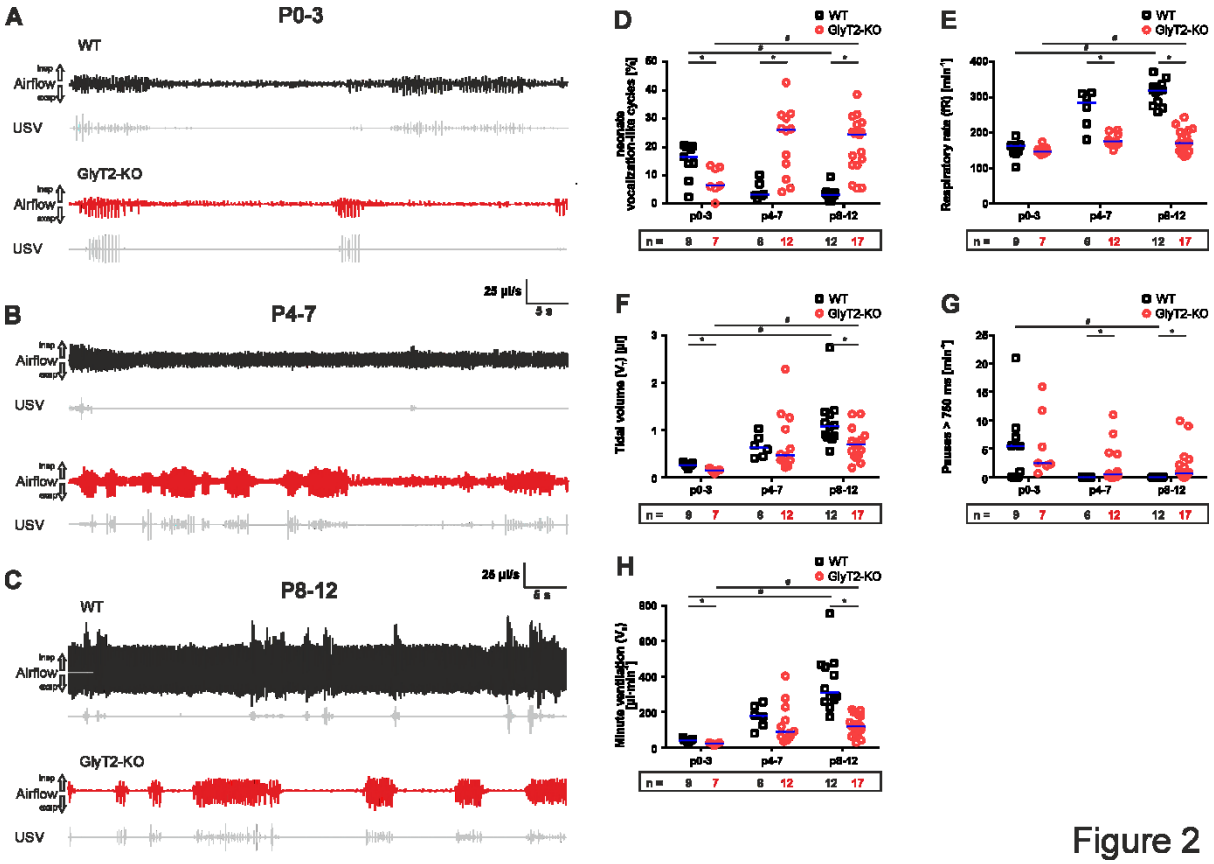

Figure 2

Figure 3:

Respiratory data corrected for body weight (BW [g]). **(A)** Respiratory rate corrected for body weight (*f*R/BW). **(B)** tidal volume corrected for body weight (T_V/BW)**. (C)** Minute ventilation corrected for body weight (V_e/BW). Subjects presented as single data point, WT black squares, GlyT2-KO red circles, median is shown by the blue line; n= number of animals. Significant differences ($p < 0.05$) between genotype per age categories are marked as "*" (Mann-Whitney U-Test). Significant differences ($p < 0.05$) between age categories are marked as "#" (Kruskal-Wallis One Way ANOVA).

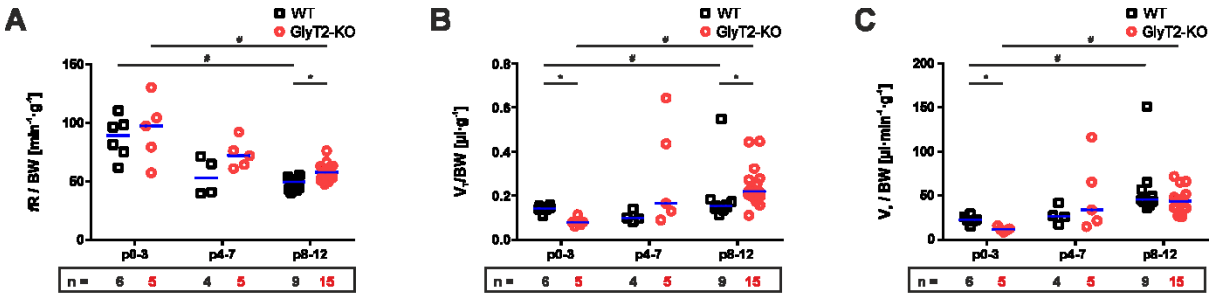

Figure 3

Figure 4:

Analysis of network activity in respiratory rhythmic slice preparation. **(A)** Schematic drawing of the slice (modified after Paxinos *et al.*, 2001). **(B)** Summary of the field potential data: burst frequency [Hz], IrrScore = irregularity score, **(C)** Analysis of calcium imaging data from images as shown in (D-I). Data points represent the average number of cells per image plane obtained from Z-stacks for each slice. **(D-F)** Data from a WT mouse, **(D)** Cross-correlation (CC) map, **(E)** EGFP-fluorescence (green), **(F)** Raw calcium signal traces from cells in panels D and E; lower trace (black): simultaneous field potential recording. **(G-I)** Representative GlyT2-KO data, **(G)** Cross-correlation (CC) map, **(H)** EGFP-fluorescence, **(I)** raw calcium signal traces from cells in panels G and H, lower trace (black): simultaneous field potential recording. Subjects presented as single data point, WT black squares, GlyT2-KO red circles, median is shown by the blue line; n= number of animals. Scale bars (panel D,E,G,H) are 40 µm.

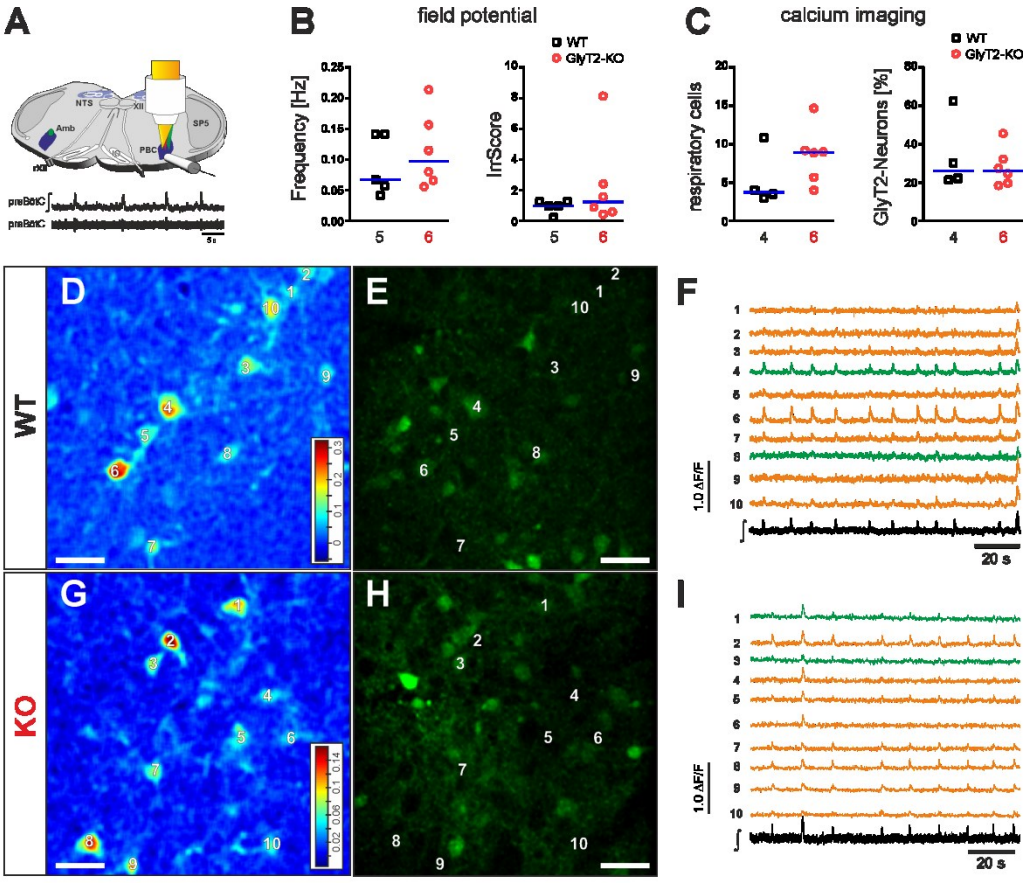

Figure 4

Figure 5:

Developmental difference in vocal activity. **(A)** Calls per minute, **(B)** Latency to start calling. Subjects presented as single data point, WT black squares, GlyT2-KO red circles, median is shown by the blue line; n= number of animals. Significant differences ($p < 0.05$) between age categories are marked as "#" (Kruskal-Wallis One Way ANOVA).

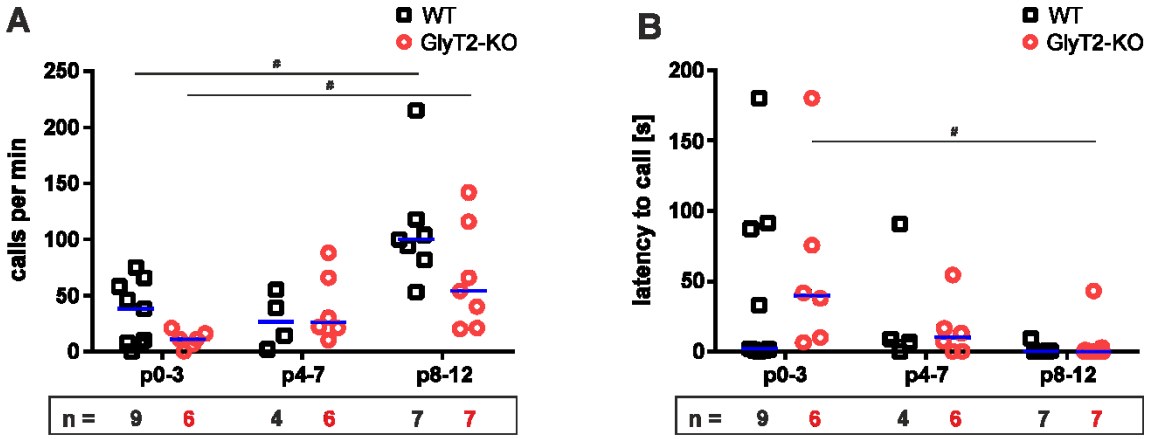

Figure 5

Figure 6: Acoustic structure of calls in WT and GlyT2-KO mice**. (A,B)** Spectrogram from a WT (A) and from a GlyT2-KO mouse (B); age group P8-12; spectrogram settings: 125 kHZ, FFT=512pt, time resolution=2ms, **(C)** Duration of USVs, **(D)** Mean peak frequency (PF) of USVs, **(E)** Frequency range of USVs, **(F)** Slope of USVs. Subjects presented as single data point, WT black squares, GlyT2-KO red circles, median is shown by the blue line; n= number of animals. Significant differences ($p < 0.05$) between genotype per age categories are marked as "*" (Mann-Whitney U-Test). Significant differences ($p < 0.05$) between age categories are marked as "#" (Kruskal-Wallis One Way ANOVA).

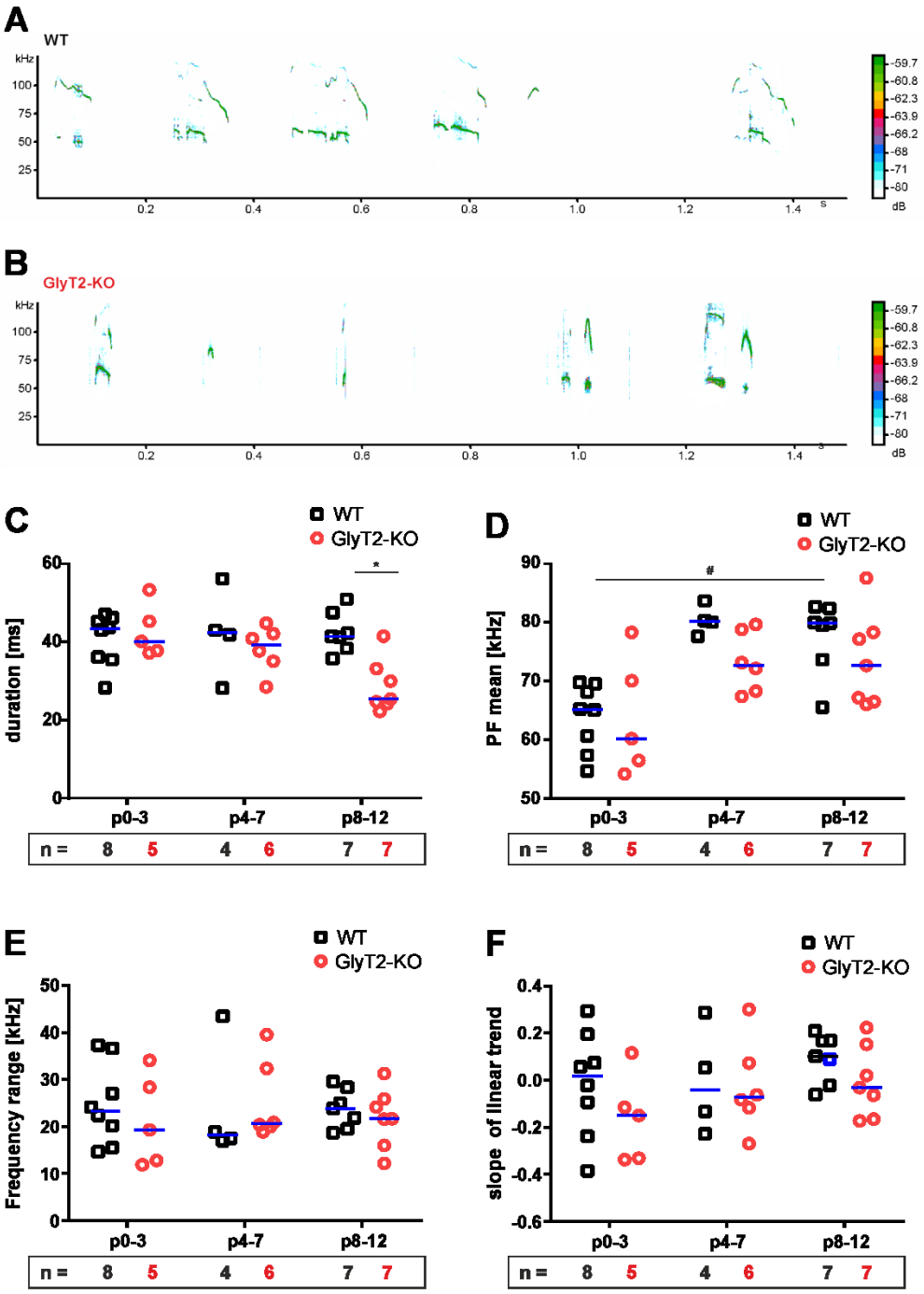

Figure 6

Figure 7:

Analysis of respiratory airflow during normal breathing and USVs. **(A)** Inspiratory peak flow from respiratory cycles that are associated with a USV call. **(B)** Inspiratory peak flow from respiratory cycles that are not associated with a USV call. **(C)** Increase of inspiratory flow associated with USV (difference of peak flow during call and no call). **(D)** Expiratory peak flow from respiratory cycles that are associated with a USV call. **(E)** Expiratory peak flow form respiratory cycles that are not associated with a USV call. **(F)** Increase of expiratory flow associated with USV (difference peak flows call /no call). Subjects presented as single data point, WT black squares, GlyT2-KO red circles, median is shown by the blue line; n= number of animals. Significant differences ($p < 0.05$) between genotype per age categories are marked as "*" (Mann-Whitney U-Test). Significant differences ($p < 0.05$) between age categories are marked as "#" (Kruskal-Wallis One Way ANOVA).

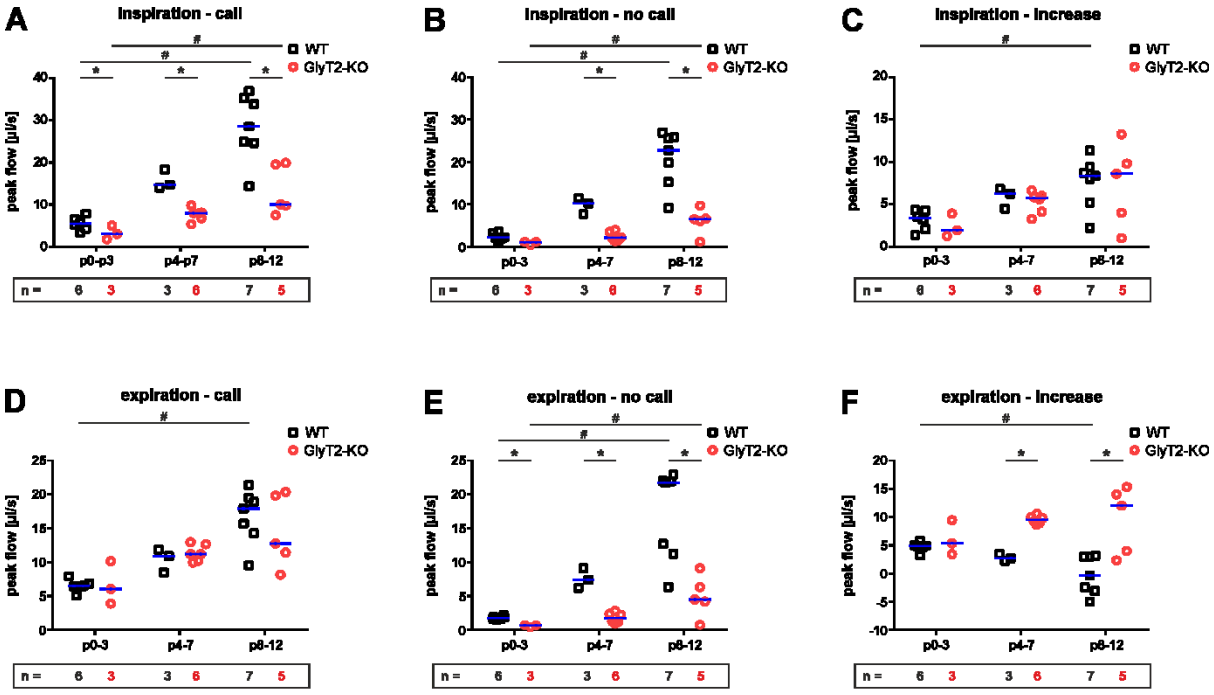

Figure 7

Figure 8:

Timing of the ultrasound signal in relation to the respiratory peak flow. **(A,B)** Respiratory airflow (upper trace) calculated volume (middle trace) and USV recording (lower trace) from a neonatal (P0-3) WT (A) and neonatal GlyT2-KO mouse (B). **(A',B')** Magnification of recordings in WT mice (A') and GlyT2-KO (B'). The gray shadows highlight the timing of the USV calls. Note that in both genotypes the USV call starts closer to the expiratory flow peak. **(C,D)** Respiratory airflow (upper trace) calculated volume (middle trace) and USV recording (lower trace) from a WT (**C**) mouse (second postnatal week (P8-12) and a symptomatic GlyT2-KO mouse (**D**). **(C',D')** Magnification of recordings in WT mice (C') and GlyT2-KO (D'). The grey shadows highlight the timing of the USV calls. Note that in WT the USVs calls start before the expiratory peak flow while in GlyT2-KO the USV calls start at the expiratory peak flow. **(E,F)** Descriptive statistics of the timing of the USV calls. **(E)** Latency to the call in respect to the zero crossing of the flow signal (peak of volume; red vertical lines in a'-d'). **(F)** Timing of the call in respect to peak expiratory flow (blue vertical lines). Subjects presented as single data point, WT black squares, GlyT2-KO red circles, median is shown by the blue line; n= number of animals. Significant differences ($p < 0.05$) between genotype per age categories are marked as "*" (Mann-Whitney U-Test). Significant differences ($p < 0.05$) between age categories are marked as "#" (Kruskal-Wallis One Way ANOVA).

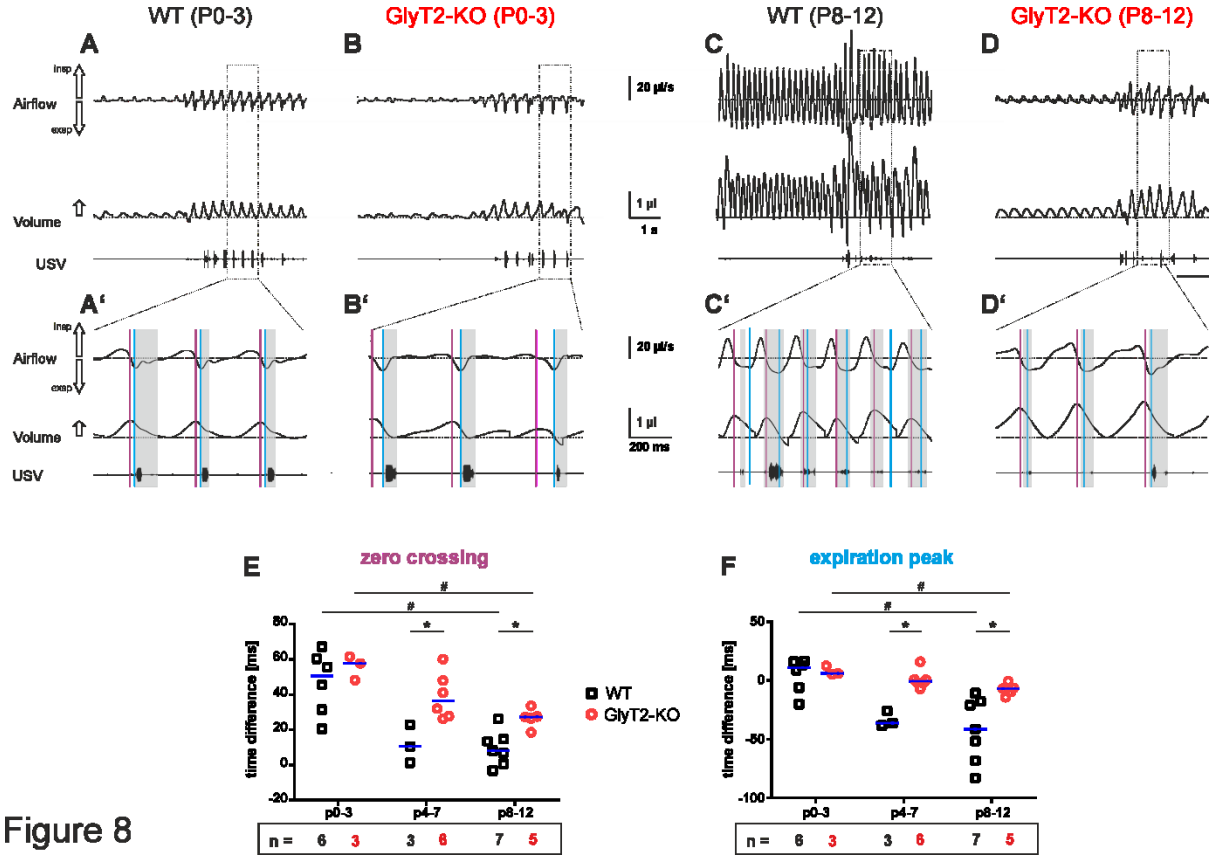

Figure 8

Table 1:

Summary of breathing parameters

	P0-3		P4-P7		P8-12		
	WT	KO	WT	KO	WT	KO	significant interaction/ violation of GLM test assumptions
Number of animal	**(n=9)**	**(n=7)**	**(n=6)**	**(n=12)**	**(n=12)**	**(n=17)**	
Neonate vocalization-like cycles [%]	**16.5 (11.1-20.1)**	**6.4* (5.5-13)**	**3.2 (2.5-7.8)**	**26.1* (10-31)**	**3.2# (1.4-3.9)**	**24.3*# (13.7-28.3)**	**yes**
Respiratory rate (*f*R) [min^{-1}]	**163 (143-167)**	**148 (141-157)**	**286 (214-310)**	**177* (168-192)**	**319# (279-336)**	**171*# (149-205)**	**yes**
Tidal-Volume (V_T) [µl]	**0.25 (0.23-0.3)**	**0.11* (0.12-0.15)**	**0.63 (0.43-8.88)**	**0.47 (0.35-1.2)**	**1.1# (0.85-1.36)**	**0.69*# (0.46-0.83)**	**yes**
Pauses > 750 ms [min^{-1}]	**5.5 (0.02-7.8)**	**2.5 (2-11.7)**	**0.0 (0.0-0.0)**	**0.46* (0.01-4.3)**	**0.0# (0.0-0.0)**	**0.65* (0.2-2.7)**	**yes**
Minute ventilation (V_e) [µl·min^{-1}]	**39.6 (34.5-44.1)**	**21.6* (18.3-26.2)**	**178 (115-237)**	**86.8 (60.7-209)**	**309# (262-464)**	**120*# (79.1-182)**	**yes**
Peak inspiratory flow [µl·s^{-1}]	**3.2 (2.7-3.4)**	**1.9* (1.6-2.2)**	**11.4 (7.5-17.6)**	**5.3 (3.9-14)**	**21.5# (17.2-28.8)**	**8.3*# (5.5-11.7)**	**yes**
Peak expiratory flow [µl·s^{-1}]	**2.5 (2.1-3.2)**	**1.2* (0.76-1.5)**	**8.3 (5.5-11.9)**	**5.8 (3.4-15.2)**	**13.6# (11-21)**	**9.3*# (4.6-11.2)**	**yes**
CV tidal volume	**1.8 (1.4-2.5)**	**1.6 (1-1.8)**	**3.7 (3-4.6)**	**1.3* (1.1-1.5)**	**3.5# (3-4.2)**	**1.5* (1.2-2)**	**yes**
CV Interval	**2.9 (2.4-4.8)**	**2.9 (2.3-4.4)**	**9.2 (7.6-10.3)**	**3.1* (1.9-5.6)**	**6.7# (6.1-7.3)**	**3.9* (2-4.7)**	**yes**
$IrrScore_{TV}$	**0.52 (0.37-2)**	**0.71 (0.6-1.3)**	**0.15 (0.12-0.19)**	**0.56* (0.33-1.3)**	**0.2# (0.17-0.22)**	**0.34*# (0.22-0.47)**	**yes**
$IrrScore_{Int}$	**0.31 (0.19-0.43)**	**0.3 (0.21-0.45)**	**0.07 (0.06-0.09)**	**0.21* (0.15-0.44)**	**0.1# (0.09-0.11)**	**0.18* (0.1-0.32)**	**yes**

Body weight (BW) [g]	**1.9 (1.6-2.2) (n=6)**	**1.6 (1.2-2.3) (n=5)**	**4.7 (4.3-6.2) (n=4)**	**2.3* (2.1-2.7) (n=5)**	**6.7# (5.9-7.2) (n=9)**	**3*# (2.7-3.7) (n=15)**	**yes**
fR / BW [$min^{-1} \cdot g^{-1}$]	**89.1 (71.8-101)**	**97.4 (68.3-117)**	**53 (40-69.9)**	**72.1 (62.9-84.3)**	**49.7# (43-52.9)**	**57.7*# (53-63.1)**	**yes**
V_T/BW [$\mu l \cdot g^{-1}$]	**0.14 (0.13-0.15)**	**0.08* (0.06-0.1)**	**0.1 (0.09-0.13)**	**0.16 (0.11-0.53)**	**0.15# (0.14-0.18)**	**0.22*# (0.2-0.27)**	**yes**
V_e / BW [$\mu l \cdot min^{-1} \cdot g^{-1}$]	**22.7 (20.2-27)**	**11.9* (10-14.4)**	**26.8 (19.7-38.2)**	**34 (18-91)**	**45.6# (41-61.2)**	**43.5# (35.1-51.8)**	**yes**

Data are shown as median and IQR. Statistical tests were two way ANOVA (see methods). Significant differences ($p < 0.05$) between genotype per age categories are marked as "*" (Mann-Whitney U-Test). Significant differences ($p < 0.05$) between age categories are marked as "#" (Kruskal-Wallis One Way ANOVA). Number of animals is referring to the number of animals tested from each strain and age group. Apneas (>750 ms) are calculated per minute. GLM: general linear model (univariate analysis of variance).

References

Anderson TM, Garcia AJ, 3rd, Baertsch NA, Pollak J, Bloom JC, Wei AD, Rai KG & Ramirez JM. (2016). A novel excitatory network for the control of breathing. *Nature* **536,** 76-80.

Anderson TM & Ramirez JM. (2017). Respiratory rhythm generation: triple oscillator hypothesis. *F1000Res* **6,** 139.

Arata A. (2009). Respiratory activity of the neonatal dorsolateral pons in vitro. *Respir Physiol Neurobiol* **168,** 144-152.

Baertsch NA, Baertsch HC & Ramirez JM. (2018). The interdependence of excitation and inhibition for the control of dynamic breathing rhythms. *Nat Commun* **9,** 843.

Barnett WH, Jenkin SEM, Milsom WK, Paton JFR, Abdala APL, Molkov YI & Zoccal DB. (2017). The Kölliker-Fuse orchestrates the timing of expiratory abdominal nerve bursting. *Journal of Neurophysiology***,** jn.00499.02017.

Barthe JY & Clarac F. (1997). Modulation of the spinal network for locomotion by substance P in the neonatal rat. *Exp Brain Res* **115,** 485-492.

Becker CM, Schmieden V, Tarroni P, Strasser U & Betz H. (1992). Isoform-selective deficit of glycine receptors in the mouse mutant spastic. *Neuron* **8,** 283-289.

Berger AJ, Dieudonne S & Ascher P. (1998). Glycine uptake governs glycine site occupancy at NMDA receptors of excitatory synapses. *J Neurophysiol* **80,** 3336-3340.

Bianchi AL, Denavit-Saubie M & Champagnat J. (1995). Central control of breathing in mammals: neuronal circuitry, membrane properties, and neurotransmitters. *Physiol Rev* **75,** 1-45.

Bogdanik LP, Chapman HD, Miers KE, Serreze DV & Burgess RW. (2012). A MusD Retrotransposon Insertion in the Mouse Slc6a5 Gene Causes Alterations in Neuromuscular Junction Maturation and Behavioral Phenotypes. *PLoS ONE* **7,** e30217.

Buckwalter MS, Cook SA, Davisson MT, White WF & Camper SA. (1994). A frameshift mutation in the mouse α1 glycine receptor gene (Gira1) results in progressive neurological symptoms and juvenile death. *Human Molecular Genetics* **3,** 2025-2030.

Busselberg D, Bischoff AM, Becker K, Becker CM & Richter DW. (2001). The respiratory rhythm in mutant oscillator mice. *Neurosci Lett* **316,** 99-102.

Cui Y, Kam K, Sherman D, Janczewski WA, Zheng Y & Feldman JL. (2016). Defining preBotzinger Complex Rhythm- and Pattern-Generating Neural Microcircuits In Vivo. *Neuron* **91,** 602-614.

Drorbaugh JE & Fenn WO. (1955). A barometric method for measuring ventilation in newborn infants. *Pediatrics* **16,** 81-87.

Dutschmann M & Herbert H. (2006). The Kölliker-Fuse nucleus gates the postinspiratory phase of the respiratory cycle to control inspiratory off-switch and upper airway resistance in rat. *European Journal of Neuroscience* **24,** 1071-1084.

Dutschmann M, Jones SE, Subramanian HH, Stanic D & Bautista TG. (2014). The physiological significance of postinspiration in respiratory control. *Prog Brain Res* **212,** 113-130.

Dutschmann M & Paton JF. (2002). Inhibitory synaptic mechanisms regulating upper airway patency. *Respir Physiolo Neurobiol* **131,** 57-63.

Eulenburg V, Armsen W, Betz H & Gomeza J. (2005). Glycine transporters: essential regulators of neurotransmission. *Trends Biochem Sci* **30,** 325-333.

Ezure K, Tanaka I & Kondo M. (2003). Glycine is used as a transmitter by decrementing expiratory neurons of the ventrolateral medulla in the rat. *J Neurosci* **23,** 8941-8948.

Feldman JL & Kam K. (2015). Facing the challenge of mammalian neural microcircuits: taking a few breaths may help. *The Journal of Physiology* **593,** 3-23.

Feng G, Tintrup H, Kirsch J, Nichol MC, Kuhse J, Betz H & Sanes JR. (1998). Dual requirement for gephyrin in glycine receptor clustering and molybdoenzyme activity. *Science* **282,** 1321-1324.

Fischer J, Hammerschmidt K, Cheney DL & Seyfarth RM. (2001). Acoustic features of female chacma baboon barks. *Ethology* **107,** 33-54.

Fischer J, Noser R & Hammerschmidt K. (2013). Bioacoustic Field Research: A Primer to Acoustic Analyses and Playback Experiments With Primates. *American Journal of Primatology* **75,** 643-663.

Fujii M, Arata A, Kanbara-Kume N, Saito K, Yanagawa Y & Obata K. (2007). Respiratory activity in brainstem of fetal mice lacking glutamate decarboxylase 65/67 and vesicular GABA transporter. *Neuroscience* **146,** 1044-1052.

Gautier H, Remmers JE & Bartlett D. (1973). Control of the duration of expiration. *Respiration Physiology* **18,** 205-221.

Gomeza J, Ohno K, Hulsmann S, Armsen W, Eulenburg V, Richter DW, Laube B & Betz H. (2003). Deletion of the mouse glycine transporter 2 results in a hyperekplexia phenotype and postnatal lethality. *Neuron* **40,** 797-806.

Graham BA, Schofield PR, Sah P & Callister RJ. (2003). Altered inhibitory synaptic transmission in superficial dorsal horn neurones in spastic and oscillator mice. *J Physiol* **551,** 905-916.

Gray PA, Janczewski WA, Mellen N, McCrimmon DR & Feldman JL. (2001). Normal breathing requires preBotzinger complex neurokinin-1 receptor-expressing neurons. *Nat Neurosci* **4,** 927-930.

Grundy D. (2015). Principles and standards for reporting animal experiments in The Journal of Physiology and Experimental Physiology. *J Physiol* **593,** 2547-2549.

Hammerschmidt K, Reisinger E, Westekemper K, Ehrenreich L, Strenzke N & Fischer J. (2012). Mice do not require auditory input for the normal development of their ultrasonic vocalizations. *BMC Neurosci* **13**.

Hammerschmidt K, Whelan G, Eichele G & Fischer J. (2015). Mice lacking the cerebral cortex develop normal song: Insights into the foundations of vocal learning. *Sci Rep* **5**.

Hernandez-Miranda LR, Ruffault P-L, Bouvier JC, Murray AJ, Morin-Surun M-P, Zampieri N, Cholewa-Waclaw JB, Ey E, Brunet J-F, Champagnat J, Fortin G & Birchmeier C. (2017). Genetic identification of a hindbrain nucleus essential for innate vocalization. *Proceedings of the National Academy of Sciences* **114,** 8095-8100.

Hodges MR, Wehner M, Aungst J, Smith JC & Richerson GB. (2009). Transgenic mice lacking serotonin neurons have severe apnea and high mortality during development. *J Neurosci* **29,** 10341-10349.

Hülsmann S, Mesuret G, Dannenberg J, Arnoldt M & Niebert M. (2016). GlyT2-dependent preservation of MECP2-expression in inhibitory neurons improves early respiratory symptoms but does not rescue survival in a mouse model of Rett syndrome. *Frontiers in Physiology* **7,** 385.

Janczewski WA & Feldman JL. (2006). Distinct rhythm generators for inspiration and expiration in the juvenile rat. *J Physiol* **570,** 407-420.

Janczewski WA, Tashima A, Hsu P, Cui Y & Feldman JL. (2013). Role of inhibition in respiratory pattern generation. *J Neurosci* **33,** 5454-5465.

Kling C, Koch M, Saul B & Becker CM. (1997). The frameshift mutation oscillator (Glra1(spd-ot)) produces a complete loss of glycine receptor alpha1-polypeptide in mouse central nervous system. *Neuroscience* **78,** 411-417.

Koch H, Garcia AJ, 3rd & Ramirez JM. (2011). Network reconfiguration and neuronal plasticity in rhythm-generating networks. *Integr Comp Biol* **51,** 856-868.

Krey RA, Goodreau AM, Arnold TB & Del Negro CA. (2010). Outward currents contributing to inspiratory burst termination in preB?tzinger Complex neurons of neonatal mice studied in vitro. *Frontiers in Neural Circuits* **4**.

Latal AT, Kremer T, Gomeza J, Eulenburg V & Hulsmann S. (2010). Development of synaptic inhibition in glycine transporter 2 deficient mice. *Mol Cell Neurosci* **44,** 342-352.

Mahrt E, Agarwal A, Perkel D, Portfors C & Elemans CP. (2016). Mice produce ultrasonic vocalizations by intra-laryngeal planar impinging jets. *Curr Biol* **26,** R880-R881.

Marchenko V, Koizumi H, Mosher B, Koshiya N, Tariq MF, Bezdudnaya TG, Zhang R, Molkov YI, Rybak IA & Smith JC. (2016). Perturbations of Respiratory Rhythm and Pattern by Disrupting Synaptic Inhibition within Pre-Bötzinger and Bötzinger Complexes. *eNeuro* **3,** ENEURO.0011-0016.2016.

Markstahler U, Kremer E, Kimmina S, Becker K & Richter DW. (2002). Effects of functional knock-out of alpha 1 glycine-receptors on breathing movements in oscillator mice. *Respir Physiolo Neurobiol* **130,** 33-42.

Mesuret G, Dannenberg J, Arnoldt M, Grützner A-A, Niebert M & Hülsmann S. (2018). Breathing disturbances in a model of Rett syndrome: A potential involvement of the glycine receptor α3 subunit? *Respiratory Physiology & Neurobiology* **248,** 43-47.

Noirot E. (1972). Ultrasounds and maternal behavior in small rodents. *Dev Psychobiol* **5,** 371-387.

Noirot E. (1974). Nest-building by the virgin female mouse exposed to ultrasound from inaccessible pups. *Animal behaviour* **22,** 410-420.

Onimaru H & Homma I. (2003). A novel functional neuron group for respiratory rhythm generation in the ventral medulla. *J Neurosci* **23,** 1478-1486.

Pagliardini S, Janczewski WA, Tan W, Dickson CT, Deisseroth K & Feldman JL. (2011). Active Expiration Induced by Excitation of Ventral Medulla in Adult Anesthetized Rats. *The Journal of Neuroscience* **31,** 2895-2905.

Paxinos G, Franklin KBJ & Franklin KBJ. (2001). *The mouse brain in stereotaxic coordinates*. Academic Press, San Diego.

Pierrefiche O, Schwarzacher SW, Bischoff AM & Richter DW. (1998). Blockade of synaptic inhibition within the pre-Botzinger complex in the cat suppresses respiratory rhythm generation in vivo. *J Physiol* **509 (Pt 1),** 245-254.

Portfors CV. (2007). Types and Functions of Ultrasonic Vocalizations in Laboratory Rats and Mice. *Journal of the American Association for Laboratory Animal Science* **46,** 28-34.

Price WM & Batsel HL. (1970). Respiratory neurons participating in sneeze and in response to resistance to expiration. *Experimental Neurology* **29,** 554-570.

Rahman J, Besser S, Schnell C, Eulenburg V, Hirrlinger J, Wojcik SM & Hulsmann S. (2015). Genetic ablation of VIAAT in glycinergic neurons causes a severe respiratory phenotype and perinatal death. *Brain Struct Funct* **220,** 2835-2849.

Ramirez JM, Quellmalz UJ & Richter DW. (1996). Postnatal changes in the mammalian respiratory network as revealed by the transverse brainstem slice of mice. *J Physiol* **491 (Pt 3),** 799-812.

Richter DW. (1982). Generation and maintenance of the respiratory rhythm. *J Exp Biol* **100,** 93-107.

Richter DW & Smith JC. (2014). Respiratory rhythm generation in vivo. *Physiology (Bethesda)* **29,** 58-71.

Schaefer N, Langlhofer G, Kluck CJ & Villmann C. (2013). Glycine receptor mouse mutants: model systems for human hyperekplexia. *British Journal of Pharmacology* **170,** 933-952.

Schnell C, Fresemann J & Hulsmann S. (2011). Determinants of functional coupling between astrocytes and respiratory neurons in the pre-Botzinger complex. *PLoS One* **6,** e26309.

Shao XM & Feldman JL. (1997). Respiratory rhythm generation and synaptic inhibition of expiratory neurons in pre-Botzinger complex: differential roles of glycinergic and GABAergic neural transmission. *J Neurophysiol* **77,** 1853-1860.

Shevtsova NA, Busselberg D, Molkov YI, Bischoff AM, Smith JC, Richter DW & Rybak IA. (2014). Effects of glycinergic inhibition failure on respiratory rhythm and pattern generation. *Prog Brain Res* **209,** 25-38.

Simpson EM, Linder CC, Sargent EE, Davisson MT, Mobraaten LE & Sharp JJ. (1997). Genetic variation among 129 substrains and its importance for targeted mutagenesis in mice. *Nature genetics* **16,** 19-27.

Smith JC, Ellenberger HH, Ballanyi K, Richter DW & Feldman JL. (1991). Pre-Botzinger complex: a brainstem region that may generate respiratory rhythm in mammals. *Science* **254,** 726-729.

Tan W, Janczewski WA, Yang P, Shao XM, Callaway EM & Feldman JL. (2008). Silencing preBotzinger Complex somatostatin-expressing neurons induces persistent apnea in awake rat. *Nat Neurosci* **11,** 538-540.

Turrigiano GG & Nelson SB. (2004). Homeostatic plasticity in the developing nervous system. *Nat Rev Neurosci* **5,** 97-107.

Vann NC, Pham FD, Hayes JA, Kottick A & Del Negro CA. (2016). Transient Suppression of Dbx1 PreBötzinger Interneurons Disrupts Breathing in Adult Mice. *PLOS ONE* **11,** e0162418.

Wegener E, Brendel C, Fischer A, Hulsmann S, Gartner J & Huppke P. (2014). Characterization of the MeCP2R168X knockin mouse model for Rett syndrome. *PLoS One* **9,** e115444.

Winter SM, Fresemann J, Schnell C, Oku Y, Hirrlinger J & Hulsmann S. (2009). Glycinergic interneurons are functionally integrated into the inspiratory network of mouse medullary slices. *Pflugers Arch* **458,** 459-469.

Winter SM, Fresemann J, Schnell C, Oku Y, Hirrlinger J & Hülsmann S. (2010). Glycinergic interneurons in the respiratory network of the rhythmic slice preparation. *Adv Exp Med Biol* **669,** 97-100.

Wojcik SM, Katsurabayashi S, Guillemin I, Friauf E, Rosenmund C, Brose N & Rhee JS. (2006). A shared vesicular carrier allows synaptic corelease of GABA and glycine. *Neuron* **50,** 575-587.

Zeilhofer HU, Studler B, Arabadzisz D, Schweizer C, Ahmadi S, Layh B, Bosl MR & Fritschy JM. (2005). Glycinergic neurons expressing enhanced green fluorescent protein in bacterial artificial chromosome transgenic mice. *J Comp Neurol* **482,** 123-141.

Zhang BY, McDonald FB, Cummings KJ, Frappell PB & Wilson RJA. (2014). Novel method for conscious airway resistance and ventilation estimation in neonatal rodents using plethysmography and a mechanical lung. *Respiratory Physiology & Neurobiology* **201,** 75-83.

Zhao MG, Hulsmann S, Winter SM, Dutschmann M & Richter DW. (2006). Calcium-regulated potassium currents secure respiratory rhythm generation after loss of glycinergic inhibition. *Eur J Neurosci* **24,** 145-154.

Additional Information

Funding

This work was funded by the Cluster of Excellence and DFG Research Center Nanoscale Microscopy and Molecular Physiology of the Brain (CNMPB). S.H. received additional support from the Deutsche Forschungsgemeinschaft DFG (Hu797/7-1, 8-1) as well as from the Volkswagen Foundation (VolkswagenStiftung).

Competing Interests

None of the authors has any conflicts of interests.

Author Contributions

The study was conceptualized by J.F., K.H. and S.H., methodology was developed and improved by J.H., K.H. and S.H., measurements were conducted by M.G.F., A.T.L., G.M., M.N., Y.O and S.H.. Formal analysis and data visualized was performed by K.H. and S.H.. All authors have critically revised and approved the final copy of the manuscript for publication. They agree to be accountable for all aspects of the work in ensuring that questions related to the accuracy or integrity of any part of the work are appropriately investigated and resolved. All persons designated as authors qualify for authorship, and all those who qualify for authorship are listed.

Acknowledgement

The authors are grateful to Anja-Annett Grützner (Göttingen) und Grit Marx (Leipzig) for technical assistance.

Swen Hülsmann is apl. Professor for Physiology at the University Medical Center Göttingen. He is leading the research group *central respiratory control* at the Clinic for Anesthesiology. His research interests are in the areas of neural control of breathing, synaptic inhibition and astrocytes.